Dalton Transactions

PAPER

View Article Online
View Journal | View Issue

Cite this: *Dalton Trans.*, 2019, **48**, 13850

Synthesis, characterization, and photoluminescence properties of three two-dimensional lanthanide-containing Dawson-type polyoxometalates†

Hechen Wu, ‡ Minna Zhi,‡ Chunli Chen, Yanhong Zhu, Pengtao Ma, * Jingping Wang and Jingyang Niu *

Received 28th June 2019,
Accepted 22nd August 2019

DOI: 10.1039/c9dt02710f

rsc.li/dalton

Three $[\alpha_2\text{-}P_2W_{17}O_{61}]^{10-}$-based lanthanide-containing polyoxometalates (LCPs) $[N(CH_3)_4]_3H_8\{Ln(H_2O)_7[Ln(H_2O)_3Ln(H_2O)_4(\alpha_2\text{-}P_2W_{17}O_{61})_2]\}\cdot 48H_2O$ [Ln = La^{3+} (**1**), Ce^{3+} (**2**), and Pr^{3+} (**3**)] were successfully obtained by the reaction of a trivacant Dawson-type precursor $[P_2W_{15}O_{56}]^{12-}$ and lanthanide ions under hydrothermal conditions. The compounds **1–3** were fully characterized by single-crystal X-ray diffraction and a series of analytical methods, including elemental analyses, powder X-ray diffraction (PXRD), IR spectroscopy, Raman spectroscopy, UV/vis diffuse reflectance spectroscopy, and thermogravimetric analysis (TGA). Single-crystal X-ray diffraction analyses indicated that **1–3** were isostructural and exhibited a 2D network architecture through the alternative connection of $[\alpha_2\text{-}P_2W_{17}O_{61}]^{10-}$ and lanthanide ions. The photoluminescence properties of **1–3** were investigated at room temperature, and **3** displayed the characteristic emissions of a Pr^{3+} emitting center, indicating that POMs can transfer energy and sensitize Pr^{3+} emissions. The reason for the weak emission intensity of Pr^{3+} emitting ions was because the radiationless losses *via* a charge-transfer Pr → W state negatively affected the emission of the Pr^{3+} ions in LCPs.

Introduction

Polyoxometalates (POMs) are large metal oxygen clusters obtained from early transition metal ions in their high oxidation states, such as V^V, Nb^V, Ta^V, Mo^{VI} and W^{VI}, which have been increasingly studied in recent years.[1] There has been a surge of interest for these state-of-the-art molecules among various scientists and industrialists due to their various properties (including well-defined molecular structures, high charge density, and hydrophilicity), thus widening their potential applications in catalysis, magnetism and optics.[2] In the large family of POMs, Keggin- and Dawson-type clusters hold a special status due to various structural types and have been well documented.[3] In comparison to Keggin-type POMs, the Dawson-type POMs have been much less reported because of the relatively difficult synthetic methods. With regard to Dawson-type POMs, a series of Dawson-based derivatives from discrete 0D to extended 3D assemblies have been obtained through the self-assembly process of POMs with metal ions and organic ligands.[4]

In the past several decades, lanthanide-containing POMs (LCPs) have been mainly studied because of their connatural diverse structures and the unique physico-chemical properties of POMs and lanthanide components, which endow them with extensive potential applications in various areas such as photoluminescence, catalysis and magnetic materials.[5] As we know, lanthanide ions exhibit a high oxophilic character with rich coordination numbers and strong coordination ability, while POMs can be regarded as good multidentate ligands owing to their oxygen-enriched nature. Accordingly, Dawson-type building blocks (including mono-, di-, tri-, and hexa-vacant Dawson POMs) can capture one or more lanthanide ions for the formation of abundant types of Dawson-type LCP derivatives in the self-assembly processes of POMs and lanthanide ions.[6]

Peacock and Weakly reported the first Dawson-type LCPs $[Ce^{III}(\alpha_2\text{-}P_2W_{17}O_{61})_2]^{17-}$ and $[Ce^{IV}(\alpha_2\text{-}P_2W_{17}O_{61})_2]^{16-}$ in 1971. Nevertheless, LCPs were only analyzed by elemental analysis and UV spectroscopy rather than by obtaining their single-crystal X-ray diffraction structure.[7] In 2001, Francesconi *et al.* obtained the complete single-crystal X-ray diffraction structure of a Dawson-type LCP $[Lu(\alpha_2\text{-}P_2W_{17}O_{61})_2]^{17-}$ and the LCP com-

Henan Key Laboratory of Polyoxometalate Chemistry, College of Chemistry and Chemical Engineering, Henan University, Kaifeng, Henan 475004, P. R. China. E-mail: mpt@henu.edu.cn, jyniu@henu.edu.cn; Fax: (+86)-371-23886876

†Electronic supplementary information (ESI) available: Materials and methods, TGA curves, IR spectroscopy, and PXRD patterns of **1–3**, 2D network architecture of **1**, emission spectra of **1**, selected bond length of **1–3**, BVS results of Ce ion in **2**. CCDC 1917530–1917532. For ESI and crystallographic data in CIF or other electronic format see DOI: 10.1039/c9dt02710f

‡These authors contributed equally to this work.

prised two $[\alpha_2\text{-}P_2W_{17}O_{61}]^{10-}$ building blocks in a *cis*-fashion.[8] Subsequently, a series of LCPs based on Dawson-type POMs were successively reported. Among the reported LCPs, most of them are discrete 0D and low-dimensional 1D structures, whereas the high-dimensional 2D and 3D structures are relatively less. In 2006, Wang and coworkers obtained three isostructural LCPs $[Ln_2(H_2O)_9(\alpha_2\text{-}P_2W_{17}O_{61})]^{4-}$ (Ln = Nd^{3+}, La^{3+}, and Eu^{3+}) under hydrothermal conditions, and these compounds showed a 2D structure built up of the 1D chains of $[Ln(H_2O)_2(\alpha_2\text{-}P_2W_{17}O_{61})]_n^{7n-}$ linked by Ln^{3+} ions. Furthermore, the photoluminescence property study indicated that Eu^{3+} ions in $[Eu_2(H_2O)_9(\alpha_2\text{-}P_2W_{17}O_{61})]^{4-}$ occupy positions with low symmetry and without an inversion center.[9] In the following year, Pope reported that the reaction of $\{P_8W_{48}\}$ with lanthanide ions under hydrothermal and conventional conditions leads to four novel LCPs with 3D structures: $Ln_4(H_2O)_{28}K_6Li_7[K\subset P_8W_{48}O_{184}(H_4W_4O_{12})_2Ln_2(H_2O)_{10}]\cdot 57H_2O$ (Ln = La^{3+}, Ce^{3+}, Pr^{3+}, and Nd^{3+}).[10] In 2010, Wang and coworkers obtained two phosphotungstate $[K_3\subset\{GdMn(H_2O)_{10}\}\{HMnGd_2(Tart)O_2(H_2O)_{15}\}\{P_6W_{42}O_{151}(H_2O)_7\}]^{11-}$ and $[K_3\subset\{GdCo(H_2O)_{11}\}_2\{P_6W_{42}O_{148}(H_2O)_7\}]^{13-}$ *via* the reactions of hexa-vacant $[H_2P_2W_{12}O_{48}]^{12-}$ units with transition metal and lanthanide ions. X-ray diffraction structural analyses indicated that $[K_3\subset\{GdMn(H_2O)_{10}\}\{HMnGd_2(Tart)O_2(H_2O)_{15}\}\{P_6W_{42}O_{151}(H_2O)_7\}]^{11-}$ has a 2D porous framework and $[K_3\subset\{GdCo(H_2O)_{11}\}_2\{P_6W_{42}O_{148}(H_2O)_7\}]^{13-}$ displays a 1D chain-like structure. Magnetic studies showed antiferromagnetic interactions in both compounds.[11] One year later, Patzke *et al.* first obtained a series of new LCPs based on an open Wells–Dawson silicotungstate anion $[\alpha\text{-}Si_2W_{18}O_{66}]^{16-}$, and the isostructural polyoxoanions $[Ln_2(H_2O)_7Si_2W_{18}O_{66}]^{10-}$ (Ln = Gd^{3+}, Tb^{3+}, Ho^{3+}) and $[Dy_2(H_2O)_{6.5}(C_2H_4O_2)_{0.5}Si_2W_{18}O_{66}]^{10-}$ showed 2D architectures. Furthermore, they also obtained another LCP $[Gd_2(H_2O)_7Si_2W_{18}O_{66}]_n^{10n-}$, and the magnetic behavior of the title compound from 2 to 300 K was found to be paramagnetic and well consistent with the spin of noninteracting gadolinium centers.[12]

In this article, we synthesized three isostructural LCPs $[N(CH_3)_4]_3H_8\{Ln(H_2O)_7[Ln(H_2O)_3Ln(H_2O)_4(\alpha_2\text{-}P_2W_{17}O_{61})_2]\}\cdot 48H_2O$ [Ln = La^{3+} (**1**), Ce^{3+} (**2**), and Pr^{3+} (**3**)] using the reaction of a trivacant Dawson-type precursor $[P_2W_{15}O_{56}]^{12-}$ and lanthanide ions under hydrothermal conditions, which was confirmed by elemental analyses, single-crystal X-ray diffraction analysis, powder X-ray diffraction (PXRD), UV/vis diffuse reflectance spectroscopy, IR spectroscopy, Raman spectroscopy, and thermogravimetric analysis (TGA). Structural analyses indicated that the title compounds displayed a 2D network structure linked by lanthanide cations. The photoluminescence properties of **1–3** were also investigated at room temperature.

Results and discussion

Structure description

The experimental PXRD patterns of **1–3** were similar and well consistent with the simulated XRD patterns from single-crystal X-ray diffraction analyses (Fig. S1†), demonstrating that compounds **1–3** were isostructural and the experimental samples of **1–3** exhibited good phase purity. It is worth noting that the peak intensities of the experimental and simulated PXRD patterns were different, which may be a result of the variation in the preferred orientation of the experimental sample during the process of recording the experimental PXRD patterns.

The isostructural architectures of **1–3** were proven by similar PXRD analyses. Herein, only the structure of **1** as a representation is described in detail. **1** crystallized in the monoclinic space group *Pn*; it comprised one fundamental polyoxoanion $\{La(H_2O)_7[La(H_2O)_3La(H_2O)_4(\alpha_2\text{-}P_2W_{17}O_{61})_2]\}^{11-}$ (Fig. 1), three $[N(CH_3)_4]^{3+}$ counter cations and forty-eight lattice water molecules, while eight H^+ protons were directly added to balance the negative charge of the anion. The added H^+ protons could not be located crystallographically and were assumed to be delocalized over the entire structure, which is a commonly observed phenomenon in the POM chemistry.[12,13]

As we know, the POM units can be further decomposed into abundant polyoxoanion fragments in a solution. In this system, two new subunits ("building block I" and "building block II") were synthesized through the self-assembly process of the $[P_2W_{15}O_{56}]^{12-}$ precursor with a $\{WO_6\}$ group and La^{3+} ions in a solution environment. As shown in Scheme 1, the La1 atom occupies the vacancy site of the $[\alpha_2\text{-}P_2W_{17}O_{61}]^{10-}$ unit for the formation of "building block I", and the La2 atom is embedded into the defect site of another $[\alpha_2\text{-}P_2W_{17}O_{61}]^{10-}$ unit to build "building block II". The La1 atom adopted a nine-coordination distorted mono-capped square antiprismatic configuration (Fig. 2a), and it was surrounded by four oxygen atoms (O27, O28, O33, O40) from the vacancy site of the $[\alpha_2\text{-}P_2W_{17}O_{61}]^{10-}$ unit, one terminal oxygen atom (O64A, symmetry code A = $+X$, $+Y$, $-1+Z$) of the adjacent $[\alpha_2\text{-}P_2W_{17}O_{61}]^{10-}$ unit, and four coordination water oxygen atoms (O1 W, O2 W, O3 W, O4 W). The bond length range of La1–O was 2.48(3)–2.76(4) Å (Table S1†). The coordination geometry around the La2 atom could be described as an eight-coordination distorted square antiprismatic configuration (Fig. 2b), which was defined by four oxygen atoms (O76, O79, O83, O87) from one $[\alpha_2\text{-}P_2W_{17}O_{61}]^{10-}$ unit, one oxygen atom (O16) from another $[\alpha_2\text{-}P_2W_{17}O_{61}]^{10-}$ unit, and three oxygen atoms

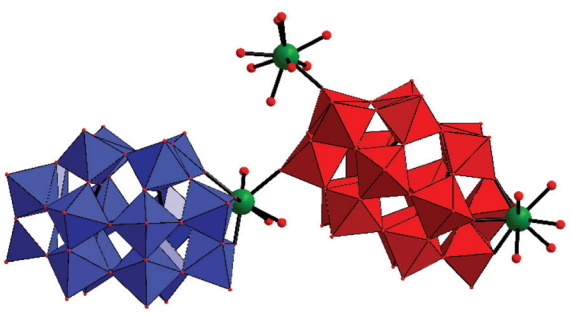

Fig. 1 Polyhedral/ball-and-stick representation of the polyoxoanion $\{La(H_2O)_7[La(H_2O)_3La(H_2O)_4(\alpha_2\text{-}P_2W_{17}O_{61})_2]\}^{11-}$ (color code: WO_6, blue and red; P, pink; La, green; O, red).

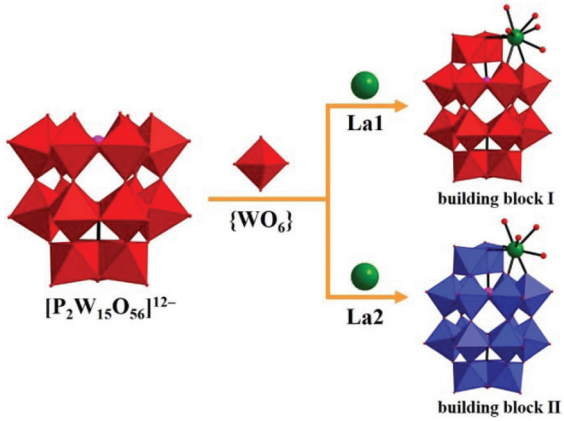

Scheme 1 The schematic synthetic process of building blocks I and II (color code: WO_6, blue and red; P, pink; La, green; O, red).

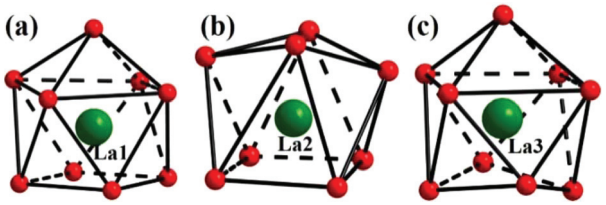

Fig. 2 (a) Coordination geometric configuration of La1; (b) coordination geometric configuration of La2; (c) coordination geometric configuration of La3.

(O5 W, O6 W, O7 W) on three coordination water molecules with the bond length of La2–O ranging from 2.43(3) to 2.63(3) Å (Table S1†). As shown in Fig. 3a, "building block I" and "building block II" are alternatively connected to construct a 1D "Z" chain-like structure through the bridging of La1 and La2 linkers. In addition, "building block I" could build another 1D linear-like architecture through the bridging of La3 atoms (Fig. 3b). The La3 atom also adopted a similar nine-coordination distorted mono-capped square antiprismatic geometry to that of the La1 atom, and their geometries could be differentiated as the La3 atom possessed a more distorted bottom plane (Fig. 2c). In the configuration of the La3 atom,

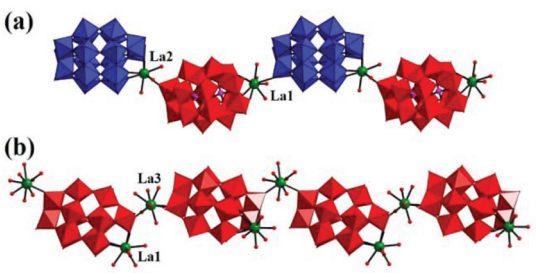

Fig. 3 (a) 1D "Z" chain of building blocks I and II through the bridging of La1 and La2 atoms; (b) 1D linear chain of building block I through the bridging of La3 atoms.

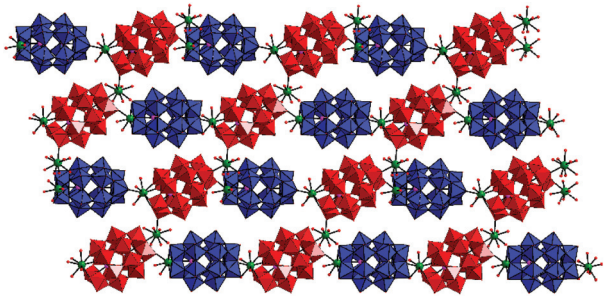

Fig. 4 The 2D network structure of the polyoxoanion of **1**.

one terminal oxygen atom (O4B, symmetry code B = 1/2 + *X*, 1 − *Y*, 1/2 + *Z*) from a $[\alpha_2\text{-}P_2W_{17}O_{61}]^{10-}$ unit, another terminal oxygen atom (O17) of the adjacent $[\alpha_2\text{-}P_2W_{17}O_{61}]^{10-}$ unit and seven oxygen atoms of water molecules (O8 W, O9 W, O10 W, O11 W, O12 W, O13 W, O14 W) together constructed a mono-capped square antiprismatic configuration with the bond length of La3–O ranging from 2.42(4) to 2.59(3) Å (Table S1†). Furthermore, the adjacent 1D "Z" chain-like structure could form a 2D network architecture connected by La3 atoms (Fig. 4), and the packing arrangement of the 2D network architecture is shown in Fig. S2.† The average bond lengths of Ln–O in **1–3** also demonstrated the presence of the lanthanide contraction effect with 2.542(4) Å, 2.528(4) Å, and 2.513(4) Å for **1**, **2** and **3**, respectively (Table S1†).

Furthermore, the other lanthanide elements were also investigated in the same solution environment and reaction conditions, and no predicted crystals were obtained. The reason may be boldly speculated that the early lanthanide elements own better coordination ability and higher coordination numbers due to the relatively larger atom radius compared with medium and heavy lanthanide elements. Especially, both the bridging La1 and La3 atoms adopted nine-coordination configurations in **1**, which may severely limit the participation of medium and heavy lanthanide atoms in constructing the isostructural 2D architecture of **1**. The results revealed that the early lanthanide atoms may prefer higher coordination numbers compared to medium and heavy lanthanide atoms: the electrostatic stability of the crystal structure decreases with the decrease in the lanthanoid atom radius as a result of the increase in ligand repulsion in the coordination sphere.[14]

In addition, Ce atoms usually exist in the valence state of +3 or +4 in complexes; hence, bond-valence-sum (BVS) calculations were used to confirm the valence state of the three Ce atoms in **2**. The calculation results revealed that all Ce atoms showed the valence state of +3 in **2** (Table S2†).

IR and Raman spectroscopies

IR and Raman spectroscopies are usually much reliable tools for confirming the composition of complexes.[15] Hence, the solid-state IR and Raman analyses of **1–3** were performed at room temperature. As shown in Fig. S3,† **1–3** have similar IR stretching bands from 400 cm^{-1} to 4000 cm^{-1}; hence, only the

IR spectrum of **1** is reported for detailed discussion. The signals at around 946, 912 and (785 and 705) cm^{-1} could be attributed to the ν(W–O_t), ν(W–O_b), and ν(W–O_c) asymmetrical vibrations of the $[\alpha_2\text{-}P_2W_{17}O_{61}]^{10-}$ POM skeleton, and the peaks appearing at 1058 and 1084 cm^{-1} were assigned to the characteristic vibrations of ν(P–O). The signals of 1400–1500 cm^{-1} were assigned to the characteristic vibrations of ν(C–N) of the $[(CH_3)_4N]^+$ cation. The vibration peaks at 1629 and 3442 cm^{-1} belonged to the bending and stretching characteristic vibrations of the O–H group in lattice and coordination water molecules, respectively. In comparison to IR spectra, the Raman spectra of **1–3** also exhibited similar characteristic peaks (Fig. 5), which provided support for the same polyoxoanion skeleton in **1–3**. The obvious characteristic Raman bands at 970, (905 and 869) and (787 and 755) cm^{-1} were attributed to the ν(W–O_t), ν(W–O_b) and ν(W–O_c) vibrations of the POM skeleton, respectively. The Raman results matched well with that of IR spectroscopy, indicating the presence of the $[\alpha_2\text{-}P_2W_{17}O_{61}]^{10-}$ skeleton in **1–3**. Both the IR and Raman spectroscopy results were consistent with the results of structural analyses.

UV/vis diffuse reflectance spectra

The UV/vis diffuse reflectance spectra of **1–3** in the range between 200 and 800 nm were recorded at room temperature (Fig. 6). All compounds **1–3** displayed a broad absorption band at about 360 nm, which may originate from the p_π–d_π charge-transfer transitions of the O → W bonds, and the band gap (E_g) could be assessed at about 2.90 eV (Fig. S4†). Another broad absorption band at around 470 nm could be found in the UV/vis diffuse reflectance spectrum of **2**, and it was likely due to the allowed 4f → 5d electron transition of the Ce^{3+} ions, demonstrating the presence of the Ce^{3+} ions in **2**. Differently, the UV/vis diffuse reflectance spectrum of **3** displays another four sharp absorption bands at 448, 470, 488 and 592 nm that arise from the $^3H_4 \rightarrow {}^3P_2$, $^3H_4 \rightarrow {}^3P_1$, $^3H_4 \rightarrow {}^3P_0$ and $^3H_4 \rightarrow {}^7D_2$ transitions of the Pr^{3+} ion, respectively, which also proves the occurrence of the Pr^{3+} ion in **3**. Obviously, no other band appeared in the diffuse reflectance spectrum of **1**, and this may be due to the completely empty 4f orbital of the La^{3+} ion, which cannot lead to the absorption bands arising from the 5d → 4f or 4f → 4f transition. Thus, the LCPs containing La^{3+} ions (like **1**) can be regarded as an ideal reference to investigate the absorption spectra of the lanthanide cations in isostructural LCPs. The results also practically indicated the existence of POM building blocks and La^{3+}, Ce^{3+}, and Pr^{3+} in **1–3**, respectively.

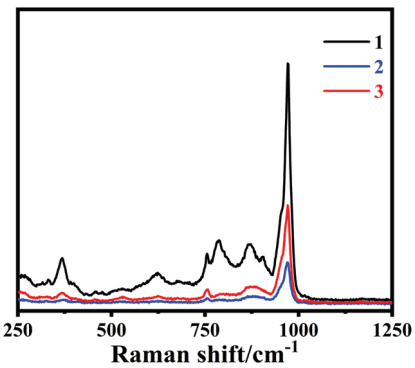

Fig. 5 Raman spectra of **1–3**.

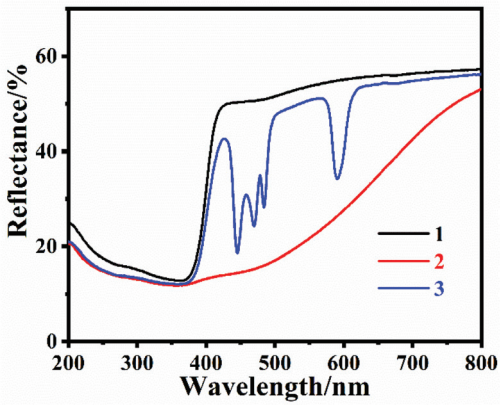

Fig. 6 The UV/vis diffuse reflectance spectra of **1–3**.

Photoluminescence properties

Lanthanide-based materials have been well studied and applied in several fields, such as lighting diodes, sensing, and bioimaging, due to their excellent luminescence characteristics, high reliability and safety.[16] The photoluminescence properties and mechanism of LCPs were studied and summarized by Yamase *et al.* as follows: first, POM components, as light-harvesting agents, were excited from the ground state $^1A_{1g}$ to the $^1T_{1u}$ state under irradiation and subsequently, the captured energy returned to the $^3T_{1u}$ state through a fast non-radiative transition; finally, the energy transfer from O → M photoexcitation $^3T_{1u}$ triplet state of ligand–metal charge transition states of POMs to lanthanide emitting ions *via* an antenna effect.[17]

According to the results of the diffuse reflectance spectra of **1–3**, the O → W charge-transfer transitions of the POM components were confirmed at approximately 360 nm. Thus, the emission spectra of **1–3** were measured under excitation at 360 nm at room temperature, and their emission spectra exhibited similar emission peaks at approximately 440 and 465 nm (Fig. 7). As is well-known, the photoluminescence emissions of the lanthanide emitting ions originate from the f–f transitions of the unfilled 4f orbitals of the lanthanide ions. Compound **1** containing La^{3+} ions exhibited a completely empty 4f orbital with no f–f transition. Hence, the emissions of **1** can be regarded as a reference to study the photoluminescence behavior of **2** and **3**. As shown in Fig. 7, the emission spectrum of **1** displays two obvious bands at 440 and 465 nm, which may be attributed to the $^1T_{1u}/^3T_{1u} \rightarrow {}^1A_{1g}$ transitions of the excited POM component, respectively.

The photoluminescence emissions of the Ce^{3+} emitting center in LCPs were studied on the basis of previously reported

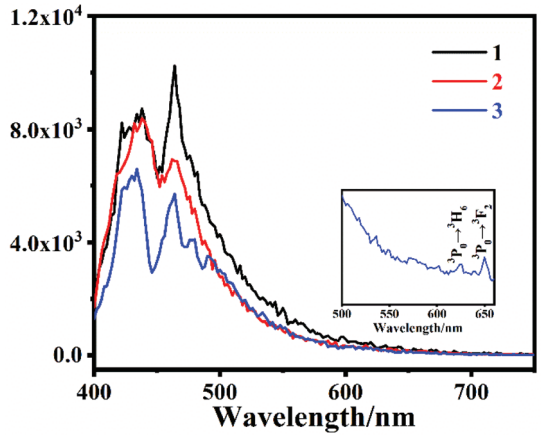

Fig. 7 The emission spectra of **1–3** (λ_{ex} = 360 nm) (inset shows the emission spectrum of **3** from 500 to 660 nm).

literature.[18] Here, the emission spectrum of **2** also shows two bands at 440 and 465 nm, and the difference between the emissions of **1** and **2** is that **2** has much lower emission intensity at 465 nm (Fig. 7), which may be due to the energy transfer from the POM components to the Ce^{3+} ions. However, it could be found that no characteristic emissions of the Ce^{3+} ions appeared in the spectrum of **2**, and this can be because the emissions of POMs completely covered the much lower 5d → 4f transition of the Ce^{3+} ions. To further demonstrate the energy transfer between POMs and Ce^{3+} ions, luminescence emission lifetimes were also recorded at the same conditions for **1** and **2**. Compared to the luminescence lifetime of **1** at 465 nm, the luminescence lifetime of **2** slightly increased from 7.15 μs to 7.51 μs (Fig. 8), indicating the potential presence of the emission of the Ce^{3+} ions and energy transfer from POMs to Ce^{3+} ions in **2**.

The UV/vis diffuse reflectance spectrum of **3** shows a broad band at 360 nm and several sharp absorption bands from 400 nm to 600 nm, and these sharp absorption bands arise directly from the excited absorption of the f–f transitions of Pr^{3+} ions. The emission spectrum of **3** was measured under excitation of 448 nm, and it exhibited four emission peaks at 527, 620, 648 and 685 nm, indicating the $P_1 \rightarrow {}^3H_5$, $^3P_0 \rightarrow {}^3H_6$, $^3P_0 \rightarrow {}^3F_2$ and $^3P_1 \rightarrow {}^3F_2$ f–f transitions belonging to the Pr^{3+} ions (Fig. S5†). Furthermore, the emission spectrum of **3** was also measured under the excitation of 360 nm to investigate the photoluminescence properties. The emission spectrum of **3** also displayed two obvious peaks at 440 and 465 nm, and the emission intensity, especially for the peak at 465 nm, was lower than that of **1**, (Fig. 7). The emission bands of the POM component partially overlapped the absorption band of the Pr^{3+} ion at 448 nm, implying that the POM component is potentially capable of transferring energy to the Pr^{3+} ion in **3**. In addition, the two shoulder peaks at 472 and 490 nm along with another two negligible peaks at 620 and 648 nm were also found in the emission spectrum of **3**, which were attributed to the characteristic $^3P_1 \rightarrow {}^3H_4$, $^3P_0 \rightarrow {}^3H_4$, $^3P_0 \rightarrow {}^3H_6$, and $^3P_0 \rightarrow {}^3F_2$ f–f transitions of Pr^{3+} emitting ions. Moreover, the luminescence lifetime of **3** at 465 nm decreased from 7.15 μs to 6.30 μs relative to the lifetime of **1** at 465 nm (Fig. 8). These above-mentioned results clearly indicate that the POM components can transfer energy to the Pr^{3+} ions and sensitize the emissions of the Pr^{3+} emitting center, while it is not easy to detect the characteristic emissions of the Pr^{3+} ions. The reason may be explained as follows: the radiationless losses *via* the charge-transfer Pr → W state severely affect the emission intensity of Pr-based LCPs.[17b]

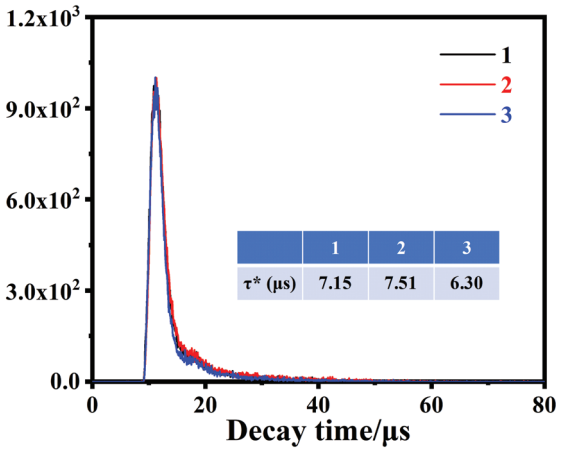

Fig. 8 The decay time diagrams of **1–3** powder samples upon excitation at 360 nm and emission at 465 nm.

Conclusion

Three isostructural LCPs $[N(CH_3)_4]_3H_8\{Ln(H_2O)_7[Ln(H_2O)_3Ln(H_2O)_4(\alpha_2\text{-}P_2W_{17}O_{61})_2]\}\cdot 48H_2O$ [Ln = La^{3+} (**1**), Ce^{3+} (**2**), and Pr^{3+} (**3**)] were successfully obtained by the reaction of the $[P_2W_{15}O_{56}]^{12-}$ precursor and lanthanide ions under hydrothermal conditions. The compounds **1–3** were structurally characterized by several physico-chemical technologies. Structural analyses showed that **1–3** displayed 2D layer-like architectures through the alternative connection of the $[\alpha_2\text{-}P_2W_{17}O_{61}]^{10-}$ building blocks and lanthanide ions, and the other lanthanide ions except La^{3+}, Ce^{3+} and Pr^{3+} could not construct the isostructural 2D architectures under the same conditions, which may be due to their relatively smaller atomic radii and lower coordination ability. The study of the UV/vis diffuse reflectance spectra of **1–3** showed the presence of the Ce^{3+} and Pr^{3+} ions in **2** and **3**, respectively, and **1** could be regarded as an ideal reference to investigate the absorption spectra of isostructural LCPs. Furthermore, the photoluminescence property study of **1–3** indicated that the POM component can transfer energy and sensitize the Ce^{3+} and Pr^{3+} emitting centers in **2** and **3**, respectively. The reason why the emission intensity of the Pr^{3+} emitting center is so weak can be explained as follows: the radiationless losses *via* the charge-transfer Pr → W state quenched the emission of the Pr^{3+} ions in LCPs.

Table 1 Crystallographic data of **1–3**

	1	**2**	**3**
Empirical formula	$C_{12}H_{168}La_3N_3O_{184}P_4W_{34}$	$C_{12}H_{168}Ce_3N_3O_{184}P_4W_{34}$	$C_{12}H_{168}N_3O_{184}P_4Pr_3W_{34}$
Formula weight	10 090.54	10 094.17	10 096.54
Temperature/K	296.15	296.15	296.15
Crystal system	Monoclinic	Monoclinic	Monoclinic
Space group	*Pn*	*Pn*	*Pn*
a [Å]	25.109(2)	25.251(3)	25.252(3)
b [Å]	14.9811(13)	15.1759(17)	15.1277(16)
c [Å]	28.785(2)	28.933(3)	28.898(3)
β [°]	105.488(2)	105.394(2)	105.3279(18)
V [Å^3]	10 434.5(15)	10 690(2)	10 646.4(19)
Z	2	2	2
ρ_{calcd} [g cm^{-3}]	2.950	2.891	2.904
μ [mm^{-1}]	19.360	18.938	19.060
F (000)	8008.0	8046.0	8052.0
Index ranges	$-23 \le h \le 29$	$-30 \le h \le 29$	$-30 \le h \le 29$
	$-17 \le k \le 17$	$-18 \le k \le 17$	$-18 \le k \le 14$
	$-33 \le l \le 34$	$-28 \le l \le 34$	$-32 \le l \le 34$
Reflections collected	52 905	53 868	53 887
Independent reflections	26 683 [R_{int} = 0.0741]	27 053 [R_{int} = 0.0770]	31 979 [R_{int} = 0.0609]
data/restraints/parameters	26 683/2558/1630	27 053/833/1627	31 979/845/1639
Goodness-of-fit on F^2	1.017	1.009	1.015
R_1, wR_2 [$I > 2\sigma(I)$]	0.0565, 0.1343	0.0597, 0.1357	0.0649, 0.1419
R_1, wR_2 [all data]	0.0789, 0.1489	0.0963, 0.1561	0.1026, 0.1649

Experimental

Synthesis

Synthesis of $[N(CH_3)_4]_3H_8\{La(H_2O)_7[La(H_2O)_3La(H_2O)_4(\alpha_2\text{-}P_2W_{17}O_{61})_2]\}\cdot 48H_2O$ (**1**). A mixture of $LaCl_3\cdot 6H_2O$ (0.185 g, 0.500 mmol), $Na_2WO_4\cdot 2H_2O$ (0.300 g, 0.900 mmol) and benzoic acid (0.006 g, 0.050 mmol) was dissolved in 20 mL distilled water and then, the mixture solution was stirred at room temperature. Two minutes later, the precursor $Na_{12}[P_2W_{15}O_{56}]\cdot 24H_2O$ (0.22 g, 0.05 mmol) was added with stirring and the pH value of the mixture solution was adjusted to approximately 4.5 by 6 mol L^{-1} NaOH solution. The solution was heated to 60 °C for 2 h. Subsequently, tetramethylammonium chloride (0.220 g, 1.000 mmol) was added and stirred for about 5 minutes at room temperature. Next, the cooled solution was moved into the reactor and heated at 120 °C for 2 days. After cooling, the solution was filtered and left for slow crystallization. Colorless block crystals were collected after about three days. Yield: 10.9% (0.480 g, based on $LaCl_3\cdot 6H_2O$ [0.185 g, 0.500 mmol]). IR (KBr, cm^{-1}): 3442 (br), 1629 (s), 1490 (s), 1084 (s), 1058 (s), 946 (s), 912 (s), 785 (s) and 705 (w). Elemental analyses calcd (%): C, 1.43; H, 1.68; N, 0.42; found, C, 1.51; H, 1.87; N, 0.35.

The synthesis of $[N(CH_3)_4]_3H_8\{Ce(H_2O)_7[Ce(H_2O)_3Ce(H_2O)_4(\alpha_2\text{-}P_2W_{17}O_{61})_2]\}\cdot 48H_2O$ (**2**) was similar to that of **1** except that $LaCl_3\cdot 6H_2O$ was replaced by $CeCl_3\cdot 6H_2O$. Finally, yellow block crystals were collected after about three days. Yield: 9.7% (0.480 g, based on $CeCl_3\cdot 6H_2O$ [0.185 g, 0.500 mmol]). IR (KBr, cm^{-1}): 3450 (br), 1620 (s), 1495 (s), 1080 (s), 1050 (s), 945 (s), 915 (s), 790 (s) and 710 (w). Elemental analyses calcd (%): C, 1.43; H, 1.68; N, 0.42; found, C, 1.53; H, 1.88; N, 0.33.

The synthesis of $[N(CH_3)_4]_3H_8\{Pr(H_2O)_7[Pr(H_2O)_3Pr(H_2O)_4(\alpha_2\text{-}P_2W_{17}O_{61})_2]\}\cdot 48H_2O$ (**3**) was similar to that of **1** except that $LaCl_3\cdot 6H_2O$ was replaced by $PrCl_3\cdot 6H_2O$. Finally, green block crystals were collected after about three days. Yield: 12.9% (0.480 g, based on $PrCl_3\cdot 6H_2O$ [0.185 g, 0.500 mmol]). IR (KBr, cm^{-1}): 3445 (br), 1620 (s), 1492 (s), 1085 (s), 1055 (s), 950 (s), 918 (s), 788 (s) and 708 (w). Elemental analyses calcd (%): C, 1.43; H, 1.68; N, 0.42; found, C, 1.48; H, 1.84; N, 0.37.

X-ray crystallography

The suitable samples of **1–3** were sealed in a glass tube and the information about X-ray diffraction degree was recorded on a Bruker APEX-II CCD diffraction meter with the graphite-monochromated Mo Kα radiation (λ = 0.71073 Å) at 296(2) K. We utilized Lorentz and polarization rectification and an applied multi-scan assimilation rectification was achieved with the SADABS scheme. Using Olex2, the frameworks of **1–3** were detected by immediate ways (SHELXS-97) and Fourier syntheses improved with the SHELXL-2018/1 refinement package applying least-squares minimization algorithm.[19] In the last step, the non-hydrogen atoms were refined anisotropically. The part of lattice water molecules was positioned by a Fourier map, and the rest was established by TGA analysis (Fig. S6†). No hydrogen atom associated with the water molecules got its position from the Fourier map. All H atoms on water molecules were straightly incorporated in the structural formula. A conclusion of the crystal information and structure refinements is summarized in Table 1.

Conflicts of interest

There are no conflicts to declare.

Acknowledgements

This work was financially supported by the National Nature Science Foundation of China (21771053, 21771054, 21571050, 21573056), Natural Science Foundation of Henan Province (132300410144 and 162300410015), Henan Province science and technology attack plan project (182102210237) and the 2018 Students Innovative Pilot Plan of Henan University (201810475016).

Notes and references

1 (*a*) P. Ma, F. Hu, J. Wang and J. Niu, *Coord. Chem. Rev.*, 2019, **378**, 281–309; (*b*) E. Cadot, M. N. Sokolov, V. P. Fedin, C. Simonnet-Jégat, S. Floquet and F. Sécheresse, *Chem. Soc. Rev.*, 2012, **41**, 7335; (*c*) J.-W. Zhao, Y.-Z. Li, L.-J. Chen and G.-Y. Yang, *Chem. Commun.*, 2016, **52**, 4418–4445; (*d*) H. Wu, R. Wan, Y. Si, P. Ma, J. Wang and J. Niu, *Dalton Trans.*, 2018, **47**, 1958–1965; (*e*) H. Wu, B. Yan, H. Li, V. Singh, P. Ma, J. Niu and J. Wang, *Inorg. Chem.*, 2018, **57**, 7665–7675; (*f*) J. Liu, Q. Han, L. Chen, J. Zhao, C. Streb and Y. Song, *Angew. Chem., Int. Ed.*, 2018, **57**, 8416–8420.

2 (*a*) T. Zhang, L. Yan, S. Cong, W. Guan and Z. Su, *Inorg. Chem. Front.*, 2014, **1**, 65–70; (*b*) D. Li, P. Ma, J. Wang and J. Niu, *Coord. Chem. Rev.*, 2019, **392**, 49–80; (*c*) Q. Han, W. Li, S. Wang, J. He and M. Li, *ChemCatChem*, 2017, **9**, 1801–1807; (*d*) Z. Shi, G. Niu, Q. Han, X. Shi and M. Li, *Mol. Catal.*, 2018, **10**, 10–18; (*e*) D. Zhang, C. Zhang, P. Ma, B. S. Bassil, R. Al-Oweini, U. Kortz, J. Wang and J. Niu, *Inorg. Chem. Front.*, 2015, **2**, 254–262; (*f*) M. Zhang, V. Singh, X. Hu, X. Ma, J. Lu, C. Zhang, J. Wang and J. Niu, *ACS Catal.*, 2019, **9**, 7641–7650; (*g*) H. Wu, M. Zhi, H. Chen, V. Singh, P. Ma, J. Wang and J. Niu, *Spectrochim. Acta, Part A*, 2019, **223**, DOI: 10.1016/j.saa.2019.117294; (*h*) Z. Lia, H. He, H. Cao, S. Sun, W. Diao, D. Gao, P. Lu, S. Zhang, Z. Guo, M. Lie, R. Liu, D. Ren, C. Liu, Y. Zhang, Z. Yang, J. Jiang and G. Zhang, *Appl. Catal., B*, 2019, **240**, 112–121; (*i*) P. Lu, Y. Yang, J. Yao, M. Wang, S. Dipazir, M. Yuan, J. Zhang, X. Wang, Z. Xie and G. Zhang, *Appl. Catal., B*, 2019, **241**, 113–119.

3 (*a*) Y.-F. Song and R. Tsunashima, *Chem. Soc. Rev.*, 2012, **41**, 7384–7402; (*b*) O. Oms, A. Dolbecq and P. Mialane, *Chem. Soc. Rev.*, 2012, **41**, 7497–7536.

4 (*a*) A. J. Howarth, T. C. Wang, S. S. Al-Juaid, S. G. Aziz, J. T. Hupp and O. K. Farha, *Dalton Trans.*, 2016, **45**, 93–97; (*b*) S. Zhang, D. Zhang, P. Ma, Y. Liang, J. Wang and J. Niu, *CrystEngComm*, 2013, **15**, 2992; (*c*) C.-C. Li, S.-X. Liu, S.-J. Li, Y. Yang, H.-Y. Jin and F.-J. Ma, *Eur. J. Inorg. Chem.*, 2012, **2012**, 3229–3234; (*d*) X. Ma, H. Li, L. Chen and J. Zhao, *Dalton Trans.*, 2016, **45**, 4935–4960; (*e*) Y. Liu, M. Jin, L. Chen and J. Zhao, *Acta Crystallogr., Sect. C: Struct. Chem.*, 2018, **C74**, 1202–1221.

5 (*a*) X. Ma, W. Yang, L. Chen and J. Zhao, *CrystEngComm*, 2015, **17**, 8175–8197; (*b*) Y. Liu, H. Li, C. Lu, P. Gong, X. Ma, L. Chen and J. Zhao, *Cryst. Growth Des.*, 2017, **17**, 3917–3928; (*c*) R. Ban, X. Sun, J. Wang, P. Ma, C. Zhang, J. Niu and J. Wang, *Dalton Trans.*, 2017, **46**, 5856–5863; (*d*) P. Ma, R. Wan, Y. Si, F. Hu, Y. Wang, J. Niu and J. Wang, *Dalton Trans.*, 2015, **44**, 11514–11523; (*e*) Q. Xu, Y. Niu, G. Wang, Y. Li, Y. Zhao, V. Singh, J. Niu and J. Wang, *Mol. Catal.*, 2018, **453**, 93–99; (*f*) C. Ritchie, V. Baslon, E. G. Moore, C. Reber and C. Boskovic, *Inorg. Chem.*, 2012, **51**, 1142–1151.

6 (*a*) P. Ma, R. Wan, Y. Wang, F. Hu, D. Zhang, J. Niu and J. Wang, *Inorg. Chem.*, 2016, **55**, 918–924; (*b*) S. Zhang, D. Zhang, P. Ma, Y. Liang, J. Wang and J. Niu, *CrystEngComm*, 2013, **15**, 2992–2998; (*c*) C. Boglio, G. Lemiere, B. Hasenknopf, S. Thorimbert, E. Lacote and M. Malacria, *Angew. Chem., Int. Ed.*, 2006, **45**, 3324–3327; (*d*) C. Boglio, G. Lenoble, C. Duhayon, B. Hasenknopf, R. Thouvenot, C. Zhang, R. C. Howell, B. P. Burton-Pye, L. C. Francesconi, E. Lacôte, S. Thorimbert, M. Malacria, C. Afonso and J.-C. Tabet, *Inorg. Chem.*, 2006, **45**, 1389–1398; (*e*) H. Li, W. Yang, Y. Chai, L. Chen and J. Zhao, *Inorg. Chem. Commun.*, 2015, **56**, 35–40; (*f*) N. Belai, M. H. Dickman, M. T. Pope, R. Contant, B. Keita, I. Mbomekalle and L. Nadjo, *Inorg. Chem.*, 2005, **44**, 169–171.

7 R. D. Peacock and T. J. R. Weakley, *J. Chem. Soc. A*, 1971, 1836–1839.

8 Q.-H. Luo, R. C. Howell, M. Dankova, J. Bartis, C. W. Williams, W. De W. Horrocks, V. G. Young, A. L. Rheingold, L. C. Francesconi and M. R. Antonio, *Inorg. Chem.*, 2001, **40**, 1894–1901.

9 Y. Lu, Y. Xu, Y. Li, E. Wang, X. Xu and Y. Ma, *Inorg. Chem.*, 2006, **45**, 2055–2060.

10 M. Zimmermann, N. Belai, R. J. Butcher, M. T. Pope, E. V. Chubarova, M. H. Dickman and U. Kortz, *Inorg. Chem.*, 2007, **46**, 1737–1740.

11 S. Yao, Z. Zhang, Y. Li, Y. Lu, E. Wang and Z. Su, *Cryst. Growth Des.*, 2010, **10**, 135–139.

12 L. Ni, F. Hussain, B. Spingler, S. Weyeneth and G. R. Patzke, *Inorg. Chem.*, 2011, **50**, 4944–4955.

13 (*a*) Q. Han, Y. Wen, J. Liu, W. Zhang, L. Chen and J. Zhao, *Inorg. Chem.*, 2017, **56**, 13228–13240; (*b*) H. Y. An, E. B. Wang, D. R. Xiao, Y. G. Li, Z. M. Su and L. Xu, *Angew. Chem., Int. Ed.*, 2006, **45**, 904–908.

14 D. G. J. Karraker, *Chem. Educ.*, 1970, **47**, 424–430.

15 (*a*) K. Dong, P. Ma, H. Wu, Y. Wu, J. Niu and J. Wang, *Inorg. Chem.*, 2019, **58**, 6000–6007; (*b*) L. Ni, H. Xu, H. Li, H. Zhao and G. Diao, *Polyhedron*, 2018, **155**, 59–65.

16 (*a*) Y. H. Kim, F. van Veggel, B. Y. Kim, S. Unithrattil, E. Kim, S.-H. Moon, J. Y. Hyun, K. H. Kim, D. Lee, J.-S. Lee and W. B. Im, *Nat. Mater.*, 2017, **16**, 543–550; (*b*) S. Li, L. Wang, D. Tang, Y. Cho, X. Liu, X. Zhou, L. Lu, L. Zhang, T. Takeda, N. Hirosaki and R.-J. Xie, *Chem. Mater.*, 2018, **30**, 494–505; (*c*) H. A. Höppe, *Angew. Chem., Int. Ed.*, 2009, **48**, 3572–3582; (*d*) S. Sivakumar, F. C. J. M. van Veggel and M. Raudsepp, *J. Am. Chem. Soc.*, 2005, **127**, 12464–12465;

(*e*) H. Wu, M. Zhi, V. Singh, H. Li, P. Ma, J. Niu and J. Wang, *Dalton Trans.*, 2018, **47**, 13949–13956; (*f*) H. Wu, H. Chen, M. Fu, R. Li, P. Ma, J. Wang and J. Niu, *Dyes Pigm.*, 2019, **171**, DOI: 10.1016/j.dyepig.2019.107696.

17 (*a*) T. Yamase, *Chem. Rev.*, 1998, **98**, 307–326; (*b*) T. Yamase, in *Handbook on the Physics and Chemistry of Rare Earths*, Elsevier, 2009, vol. 39, pp. 297–356.

18 (*a*) H. Wu, X. Meng, R. Wan, P. Ma, J. Wang and J. Niu, *Inorg. Chem. Commun.*, 2018, **95**, 154–157; (*b*) H. Zhang, X. Li, L. Zhang, Y. Zhou, X. Ren and M. Liu, *J. Alloys Compd.*, 2018, **749**, 229–235.

19 (*a*) G. M. Sheldrick, *Acta Crystallogr., Sect. C: Struct. Chem.*, 2015, **C71**, 3–8; (*b*) *A.* L. Spek, *Acta Crystallogr., Sect. C: Struct. Chem.*, 2015, **C71**, 9–18.